FPGA based Continuous Control Set Model Predictive Current Control for PMSM System Using Multi-step Error Tracking Technique

***Abstract*—To optimize the performance of the conventional continuous control set model-based predictive current control (CCS-MPCC), an extended surface mounted permanent magnet synchronous motor (SPMSM) model based multi-step error tracking CCS-MPCC (MSET-CCSMPCC) is proposed in this paper. Firstly, a traditional CCS-MPCC is derived on the basis of the conventional SPMSM model and its robustness is analyzed by considering the parameter mismatches. Secondly, the extended SPMSM model is given by incorporating the lumped disturbances into one disturbance part. Thirdly, a fast terminal sliding mode disturbance observer (FTSMDO) is designed and applied in the d- and q- axes respectively to track the disturbances fast and accurately. Fourthly, by compensating the extended SPMSM model for the estimated d- and q- axes disturbances, an EXM-CCSMPCC is designed. Fifthly, to reduce the overshoot of the EXM-CCSMPCC in the step response test, an extended SPMSM model based single step error tracking CCS-MPCC (SSET-CCSMPCC) is proposed. Sixthly, an MSET-CCSMPCC is put forward to further improve the dynamic response and steady-state performances. Experiments were carried out on a field programmable gate array (FPGA) based hardware system, and the results verified the excellent performances of the proposed methods.**

***Index Terms*—permanent magnet synchronous machine (PMSM), model-based predictive current control (MPCC), fast terminal sliding mode disturbance observer (FTSMDO), multi-step error tracking.**

I. Introduction

PERMANENT magnet synchronous motor (PMSM) has been widely employed in the industrial fields, such as textile and printing machinery, air compressor, sizing machines, owning to its superior performances [1], [2]. Digitally controlled systems are required for high-performance PMSM operations, which largely prompt the efficiency and precision. Field oriented control (FOC) is one of the most popular digital control methods applied in the industry, which can independently control the torque and magnetizing flux [3].

In a classical FOC method, the inner current control loop determines the dynamic and steady-state performances of the stator current. In addition to the traditional proportional-integral (PI) control [4], many advanced current control methods have been proposed to improve the performances of the stator current, such as deadbeat-based predictive current control (DPCC) [5], [6], model-based predictive current control (MPCC) [7], [8], hysteresis current control [9] and so on. Among these methods, MPCC is one of the most popular strategies for current control, due to its fast dynamic response and superior robustness [10]. The finite control set MPCC (FCS-MPCC) determines the optimal voltage vector by minimizing the predefined cost index. Although an excellent transient performance is achieved, the FCS-MPCC causes large current and torque ripples [11]. The continuous control set MPCC (CCS-MPCC), which is an important branch of MPCC, calculates the voltage reference by minimizing the predefined cost index. The derived voltage reference is translated into switching signals by space vector pulse-width modulation (SVPWM). Comparing with FCS-MPCC, CCS-MPCC causes smaller current ripples and requires less computation efforts [11].

Surface mounted permanent magnet synchronous motor (SPMSM) is a nonlinear and strong coupling control system where system parameter mismatches and external disturbances are inevitable, and deteriorate the performances of control algorithms. Disturbance observer (DO)-based control is one of the most effective anti-disturbance methods [12]-[18]. The paper [12] has proposed a framework, where a comprehensive DO is designed to estimate multiple disturbances. A discrete Luenberger DO is designed to improve the robustness against parameter variations in [13], and as a result a high-performance current control is achieved. Luenberger observer which is a kind of linear observer, is widely used due to its intuitive structure. However, the Luenberger observer is sensitive to parameter variations, which results in inaccurate state estimation [14]. To solve this problem, nonlinear DOs have received more and more attentions. Sliding mode observer (SMO) is one kind of the most popular nonlinear observers which is employed in a lot of high performance SPMSM drives [15]-[18]. Lumped disturbances estimated by the SMO are fed forward to compensate the sliding mode controller in [15]. A lot of researches have been done on the well-known chattering problem in the traditional SMO, which may cause high-frequency dynamics [16]. Paper [17] has proposed a sliding-mode reaching law, which reduces chatter while maintaining robust tracking performance. A unified high-order SMO (HSMO) has been designed in [18], which effectively reduces chatter.

In this paper, an extended SPMSM model based multi-step error tracking CCS-MPCC (MSET-CCSMPCC) is proposed. The conventional CCS-MPCC is characterized by fast dynamic response and small current ripples. However, it is sensitive to the parameter mismatches, which may induce steady-state error. In this work, an extended SPMSM model is given by incorporating the external disturbances and parameter variations into a disturbance part. To track the disturbance fast and accurately, a fast terminal sliding mode disturbance observer (FTSMDO) is designed. Based on the extended SPMSM model, an EXM-CCSMPCC which improves the robustness against lumped disturbances is derived. For most industrial

applications, the proposed EXM-CCSMPCC exhibits high performances on dynamic response and steady-state. However, there is overshoot in the step response test, which limits its use. To solve the problem, an MSET-CCSMPCC is proposed finally, which reduces the overshoot while keeping excellent steady-state and dynamic response performances. Experiments were carried out on a field programmable gate array (FPGA) based hardware system to verify the proposed methods.

The paper is structured as follows. In Section II, a conventional CCS-MPCC is derived on the basis of the classical SPMSM model. In Section III, an extended SPMSM model is presented by considering the lumped disturbances, and an FTSMDO is designed to estimate the disturbance part of the model. Then, an extended SPMSM model based CCS-MPCC (EXM-CCSMPCC) is proposed. To reduce the overshoot of the EXM-CCSMPCC in the step response test, a single step error tracking CCS-MPCC (SSET-CCSMPCC) is derived by assuming the error between the given current and feedback current to converge exponentially. Finally, an MSET-CCSMPCC is proposed to further improve the performances. In Section IV, experiments were carried out on a FPGA based hardware system and the results are presented and analyzed. At last, the conclusions are drawn in Section V.

II. PMSM MODEL AND CONVENTIONAL CCS-MPC

A. Modeling of The SPMSM

In synchronous rotating frame, the current equations of a SPMSM can be denoted as [19]:

$$\begin{cases} \dot{i}_d = \dfrac{1}{L}(u_d - Ri_d + Lp\omega_m i_q) \\ \dot{i}_q = \dfrac{1}{L}(u_q - Ri_q - Lp\omega_m i_d - \psi_r p\omega_m) \end{cases} \tag{1}$$

where u_d and u_q mean the stator voltages of the d- and q- axes, L is the stator inductance, R is the stator resistance, i_d and i_q are the stator currents of the d- and q- axes, ψ_r is the permanent magnet flux linkage, p is the number of pole pairs, ω_m is the rotor angular velocity.

B. Conventional CCS-MPCC

According to Euler formula, (1) can be discretized as

$$\begin{cases} i_d(t+1) = i_d(t) + \dfrac{T_c}{L}(u_d(t) - Ri_d(t) \\ \qquad +Lp\omega_m(t)i_q(t)) \\ i_q(t+1) = i_q(t) + \dfrac{T_c}{L}(u_q(t) - Ri_q(t) \\ \qquad -Lp\omega_m(t)i_d(t) - \psi_r p\omega_m(t)) \end{cases} \tag{2}$$

where T_c is the current loop control period.

The cost index of the CCS-MPC is defined as

$$J(t) = (i_d^*(t+1) - i_d(t+1))^2 + \lambda(i_q^*(t+1) - i_q(t+1))^2 \tag{3}$$

To optimize the control object, $J(t)$ in (3) is minimized by calculating appropriate voltage variables $u_d(t)$ and $u_q(t)$, which yields

$$\begin{cases} \dfrac{\partial J(t)}{\partial u_d(t)} = 0 \\ \dfrac{\partial J(t)}{\partial u_q(t)} = 0 \end{cases} \tag{4}$$

By solving the simultaneous (2), (3) and (4), the optimized voltage variables $u_d(t)$ and $u_q(t)$ are obtained.

$$\begin{cases} u_d(t) = L\dfrac{i_d^*(t+1) - i_d(t)}{T_c} + Ri_d(t) - Lp\omega_m(t)i_q(t) \\ u_q(t) = L\dfrac{i_q^*(t+1) - i_q(t)}{T_c} + Ri_q(t) + Lp\omega_m(t)i_d(t) \\ \qquad + \psi_r p\omega_m(t) \end{cases} \tag{5}$$

Parameter Sensitivity Analysis: Assume $R_v = R_n + R_\delta$, $L_v = L_n + L_\delta$, $\psi_{rv} = \psi_{rn} + \psi_{r\delta}$, where R_δ, L_δ and $\psi_{r\delta}$ are the parameter variations, R_n, L_n and ψ_{rn} are the nominal parameter values. Applying R_v, L_v and ψ_{rv} to (5), it derives

$$\begin{cases} u_{d\delta}(t) = L_n\dfrac{i_d^*(t+1) - i_d(t)}{T_c} + R_n i_d(t) \\ \qquad - L_n p\omega_m(t)i_q(t) + \Delta u_d(t) \\ u_{q\delta}(t) = L_n\dfrac{i_q^*(t+1) - i_q(t)}{T_c} + R_n i_q(t) \\ \qquad + L_n p\omega_m(t)i_d(t) + \psi_{rn}p\omega_m(t) + \Delta u_q(t) \end{cases} \tag{6}$$

Where $\Delta u_d(t) = L_\delta\frac{i_d^*(t+1) - i_d(t)}{T_c} + R_\delta i_d(t) - L_\delta p\omega_m(t)i_q(t)$, $\Delta u_q(t) = L_\delta\frac{i_q^*(t+1) - i_q(t)}{T_c} + R_\delta i_q(t) + L_\delta p\omega_m(t)i_d(t) + \psi_{r\delta}p\omega_m(t)$. Substituting (6) into (2), it derives

$$\begin{cases} i_d(t+1) = i_d^*(t+1) + \Delta u_d(t)\dfrac{T_c}{L_n} \\ i_q(t+1) = i_q^*(t+1) + \Delta u_q(t)\dfrac{T_c}{L_n} \end{cases} \tag{7}$$

From (7), it can be found that errors between the reference currents and the feedback currents are induced by the parameter mismatches. In the following section, improved CCS-MPCC methods are proposed to track the currents accurately.

III. EXTENDED SPMSM MODEL AND PROPOSED CCS-MPCC

A. Extended SPMSM Model

Regard $n_d = \frac{u_d}{L} - \frac{u_d^*}{L} - \frac{Ri_d}{L} + p\omega_m i_q$, $n_q = \frac{u_q}{L} - \frac{u_q^*}{L} - \frac{Ri_q}{L} - p\omega_m i_d - \frac{\psi_r p\omega_m}{L}$ as the lumped disturbances of d- and q- axes respectively, and the current equations of a SPMSM are denoted as

$$\begin{cases} \dot{i}_d = \dfrac{u_d^*}{L} + n_d \\ \dot{n}_d = a_d \end{cases} \tag{8}$$

$$\begin{cases} \dot{i}_q = \dfrac{u_q^*}{L} + n_q \\ \dot{n}_q = a_q \end{cases} \tag{9}$$

where u_d^* and u_q^* are the voltage references to d- and q- axes, a_d and a_q are the variation rates of the lumped disturbances.

B. Fast Terminal Sliding Mode Disturbance Observer Design

To track the lumped disturbances, an FTSMDO can be designed as

$$\begin{cases} \dot{\hat{i}}_d = \dfrac{u_d^*}{L} + \hat{n}_d + N_{d0} \\ \dot{\hat{n}}_d = N_{d1} \end{cases} \tag{10}$$

$$\begin{cases} \dot{\hat{i}}_q = \dfrac{u_q^*}{L} + \hat{n}_q + N_{q0} \\ \dot{\hat{n}}_q = N_{q1} \end{cases} \tag{11}$$

By subtracting (8) to (10) and (9) to (11), the system error state equations are derived as

$$\begin{cases} \dot{e}_d = e_{nd} - N_{d0} \\ \dot{e}_{nd} = a_d - N_{d1} \end{cases} \tag{12}$$

$$\begin{cases} \dot{e}_q = e_{nq} - N_{q0} \\ \dot{e}_{nq} = a_q - N_{q1} \end{cases} \tag{13}$$

where $e_d = i_d - \hat{i}_d$, $e_{nd} = n_d - \hat{n}_d$, $e_q = i_q - \hat{i}_q$, $e_{nq} = n_q - \hat{n}_q$

To obtain finite-time convergence and good tracking accuracy, the FTSMDO surfaces are given as

$$\begin{cases} s_d = \dot{e}_d + \alpha_d e_d + \beta_d \left|e_d\right|^{\gamma_d} \operatorname{sign}(e_d) = 0 \\ s_{nd} = \dot{e}_{nd} + \alpha_{nd} e_{nd} + \beta_{nd} \left|e_{nd}\right|^{\gamma_{nd}} \operatorname{sign}(e_{nd}) = 0 \end{cases} \tag{14}$$

$$\begin{cases} s_q = \dot{e}_q + \alpha_q e_q + \beta_q \left|e_q\right|^{\gamma_q} \operatorname{sign}(e_q) = 0 \\ s_{nq} = \dot{e}_{nq} + \alpha_{nq} e_{nq} + \beta_{nq} \left|e_{nq}\right|^{\gamma_{nq}} \operatorname{sign}(e_{nq}) = 0 \end{cases} \tag{15}$$

Where $\alpha_d > 0$, $\beta_d > 0$, $0 < \gamma_d < 1$, $\alpha_{nd} > 0$, $\beta_{nd} > 0$, $0 < \gamma_{nd} < 1$, $\alpha_q > 0$, $\beta_q > 0$, $0 < \gamma_q < 1$, $\alpha_{nq} > 0$, $\beta_{nq} > 0$, $0 < \gamma_{nq} < 1$.

Substituting (12) to (14) and (13) to (15), and considering e_{nd}, e_{nq}, a_d and a_q as the disturbances of control functions, the FTSMDO control functions can be derived as

$$\begin{cases} N_{d0} = \alpha_d e_d + \beta_d \left|e_d\right|^{\gamma_d} \operatorname{sign}(e_d) \\ N_{d1} = \alpha_{nd} e_{nd} + \beta_{nd} \left|e_{nd}\right|^{\gamma_{nd}} \operatorname{sign}(e_{nd}) \end{cases} \tag{16}$$

$$\begin{cases} N_{q0} = \alpha_q e_q + \beta_q \left|e_q\right|^{\gamma_q} \operatorname{sign}(e_q) \\ N_{q1} = \alpha_{nq} e_{nq} + \beta_{nq} \left|e_{nq}\right|^{\gamma_{nq}} \operatorname{sign}(e_{nq}) \end{cases} \tag{17}$$

The d-axis FTSMDO is analyzed as follows, and the results are also applicable to the q-axis FTSMDO.

1) *Stability of the observer* : A Lyapunov function is constructed as $V_d = \frac{1}{2} s_d^2$. Its time derivative is given as

$$\dot{V}_d = s_d \dot{s}_d \tag{18}$$

Combining the first equation of (12), (14) and (16), the surface s_d can be derived as

$$s_d = e_{nd} \tag{19}$$

According to (19) and the second equation of (12), the derivative of s_d with respect to time is

$$\dot{s}_d = a_d - N_{d1} \tag{20}$$

Then, substituting (19) and (20) to (18), $\dot{V}_d$ can be calculated as

$$\dot{V}_d = a_d s_d - N_{d1} s_d \tag{21}$$

Substitute the second equation of (16) to (21), and the $\dot{V}_d$ can be derived as

$$\begin{aligned} \dot{V}_d &= a_d s_d - (\alpha_{nd} s_d^2 + \beta_{nd} \left|s_d\right|^{\gamma_{nd}} \left|s_d\right|) \\ &\le \left|s_d\right| (\left|a_d\right| - \alpha_{nd} \left|s_d\right| - \beta_{nd} \left|s_d\right|^{\gamma_{nd}}) \end{aligned} \tag{22}$$

Therefore, when $\left|a_d\right| < \alpha_{nd} \left|s_d\right| + \beta_{nd} \left|s_d\right|^{\gamma_{nd}}$, it obtains $\dot{V}_d < 0$ ($s_d \neq 0$). Considering the control period of the current loop is so short that a_d can be regarded as zero, $\dot{V}_d < 0$ ($s_d \neq 0$) is drawn when $\alpha_{nd} > 0$ and $\beta_{nd} > 0$. So, according to the Lyapunov stability theorem, the FTSMDO surface is reached in a finite time and stay on it thereafter. The following equation is obtained accordingly.

$$\dot{e}_d = -\alpha_d e_d - \beta_d \left|e_d\right|^{\gamma_d} \operatorname{sign}(e_d) \tag{23}$$

Assuming the initial e_d does not stay at zero and the γ_d is well chosen, $e_d = 0$ can be reached in a finite time. According to (23), the physical interpretation can be depicted as:

- If e_d stays far away from zero, it obtains $\dot{e}_d \approx -\alpha_d e_d$, which means the e_d converges exponentially.
- If e_d stays close to zero, it obtains $\dot{e}_d \approx -\beta_d \left|e_d\right|^{\gamma_d} \operatorname{sign}(e_d)$, which becomes a terminal attractor.

By substituting $e_d = 0$ into (23), it obtains $e_d = \dot{e}_d = 0$, which means the designed FTSMDO has the properties of the HSMO [20]. From (19), e_{nd} vanishes to zero with time as well as s_d.

2) *Reaching time of* e_d: By solving (23), the precise time to arrive at $e_d = 0$ can be derived as

$$t_d = \frac{1}{\alpha_d (1 - \gamma_d)} \ln \frac{\alpha_d \left|e_d(0)\right|^{1-\gamma_d} + \beta_d}{\beta_d} \tag{24}$$

3) *Calculation of* $\dot{e}_d$: Let $\dot{e}_d = z$. In common, z is calculated as $z \approx \frac{1}{T_c}(e_d(t) - e_d(t-1))$, which is sensitive to the noise [21]. To improve the quality of $\dot{e}_d$, a sliding-mode differentiator (SMD) is given as follows [22].

$$\begin{cases} \dot{\hat{e}}_d = \hat{z} - l_{d0} \operatorname{sign}(\hat{e}_d - e_d) - l_{d1}(\hat{e}_d - e_d) \\ \dot{\hat{z}} = -l_{d2} \operatorname{sign}(\hat{e}_d - e_d) - l_{d3}(\hat{e}_d - e_d) \end{cases} \tag{25}$$

where $\hat{e}_d$ is the estimated value of e_d, $\hat{z}$ is the derivative of $\hat{e}_d$, which derives $z \approx \hat{z}$, $l_{d0} > 0$, $l_{d1} > 0$, $l_{d2} > 0$, $l_{d3} > 0$.

C. Extended SPMSM Model based CCS-MPCC

Substitude the estimated $\hat{n}_d$, $\hat{n}_q$ to the extended SPMSM model, and it can be rewritten as

$$\begin{cases} \dot{i}_d = \dfrac{u_d^*}{L} + \hat{n}_d \\ \dot{i}_q = \dfrac{u_q^*}{L} + \hat{n}_q \end{cases} \tag{26}$$

(26) can be discretized as

$$\begin{cases} i_d(t+1) = i_d(t) + T_c(\dfrac{u_d^*(t)}{L} + \hat{n}_d(t)) \\ i_q(t+1) = i_d(t) + T_c(\dfrac{u_q^*(t)}{L} + \hat{n}_q(t)) \end{cases} \tag{27}$$

The cost index of the EXM-CCSMPCC is defined as

$$\begin{aligned} J_e(t) =&(i_d^*(t+1) - i_d(t+1))^2 \\ &+ \lambda(i_q^*(t+1) - i_q(t+1))^2 \end{aligned} \tag{28}$$

The cost index $J_e(t)$ in (28) is minimized by calculating appropriate voltage variables $u_d^*(t)$ and $u_q^*(t)$, which yields

$$\begin{cases} \dfrac{\partial J_e(t)}{\partial u_d^*(t)} = 0 \\ \dfrac{\partial J_e(t)}{\partial u_q^*(t)} = 0 \end{cases} \tag{29}$$

By solving the simultaneous (27), (28) and (29), the optimized voltage variables $u_d^*(t)$ and $u_q^*(t)$ are derived as

$$\begin{cases} u_d^*(t) = L\dfrac{i_d^*(t+1) - i_d(t)}{T_c} - L\hat{n}_d(t) \\ u_q^*(t) = L\dfrac{i_q^*(t+1) - i_q(t)}{T_c} - L\hat{n}_q(t) \end{cases} \tag{30}$$

Fig. 1 shows the diagram of the EXM-CCSMPCC. The cost index of the proposed EXM-CCSMPCC is constructed to achieve the fastest tracking, and as a result, the i_d and i_q track the i_d^* and i_q^* as fast as possible. However, serious overshoot occurs in the step response test by using the EXM-CCSMPCC. To eliminate the overshoot, a new cost index is constructed in the next section.

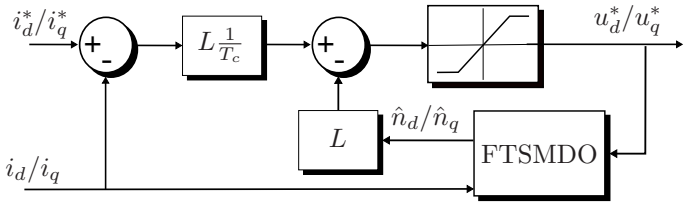

Fig. 1. Block diagram of the EXM-CCSMPCC.

D. Extended SPMSM Model based Single Step Error Tracking CCS-MPCC

Let

$$\begin{cases} \Delta_d = i_d^* - i_d \\ \Delta_q = i_q^* - i_q \end{cases} \tag{31}$$

Assume the errors between the given currents and the predicted currents converge exponentially, namely $\Delta_d = e^{-\rho_d t}$, $\Delta_q = e^{-\rho_q t}$. The time derivatives of Δ_d and Δ_q can be derived as

$$\begin{cases} \dot{\Delta}_d = -\rho_d \Delta_d \\ \dot{\Delta}_q = -\rho_q \Delta_q \end{cases} \tag{32}$$

Let $\eta_d = (1 - T_c\rho_d)$ and $\eta_q = (1 - T_c\rho_q)$, and (32) can be discretized as

$$\begin{cases} \Delta_d(t+1) = \eta_d \Delta_d(t) \\ \Delta_q(t+1) = \eta_q \Delta_q(t) \end{cases} \tag{33}$$

Where $0 < \eta_d < 1$, $0 < \eta_q < 1$.

Therefore, the cost index of the SSET-CCSMPCC is designed as

$$\begin{aligned} J_\Delta(t) = &\lambda_{d0}(\Delta_d(t)\eta_d - \Delta_d(t+1))^2 \\ &+ \lambda_{q0}(\Delta_q(t)\eta_q - \Delta_q(t+1))^2 \end{aligned} \tag{34}$$

If the cost function $J_\Delta(t)$ in (34) is minimized, (32) is approximately satisfied. Thus the Δ_d and Δ_q converge exponentially.

According to (31), it obtains

$$\begin{cases} \Delta_d(t) = i_d^*(t) - i_d(t) \\ \Delta_q(t) = i_q^*(t) - i_q(t) \\ \Delta_d(t+1) = i_d^*(t+1) - i_d(t+1) \\ \Delta_q(t+1) = i_q^*(t+1) - i_q(t+1) \end{cases} \tag{35}$$

Substituting (27) and (35) into (34), and sloving $\frac{\partial J_\Delta(t)}{\partial u_d^*(t)} = 0$, $\frac{\partial J_\Delta(t)}{\partial u_q^*(t)} = 0$, it obtains

$$\begin{cases} u_d^*(t) = \dfrac{L}{T_c}(i_d^*(t+1) - \eta_d i_d^*(t) \\ \qquad\qquad -(1-\eta_d)i_d(t)) - T_c\hat{n}_d(t)) \\ u_q^*(t) = \dfrac{L}{T_c}(i_q^*(t+1) - \eta_q i_q^*(t) \\ \qquad\qquad -(1-\eta_q)i_q(t)) - T_c\hat{n}_q(t)) \end{cases} \tag{36}$$

Fig. 2 shows the block diagram of the SSET-CCSMPCC. In the step response test, large η_d, η_q will eliminate the overshoots of the i_d and i_q, but increase the tracking time and the current ripples. To solve the problem, an MSET-CCSMPCC is proposed in the next section.

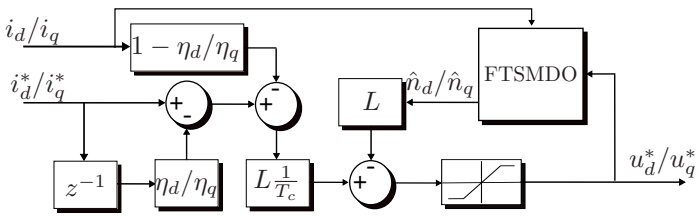

Fig. 2. Block diagram of the SSET-CCSMPCC.

E. Extended SPMSM Model based Multi-step Error Tracking CCS-MPCC

According to (33), it derives

$$\begin{cases} \Delta_d(t+1) = \eta_d^{j+1}\Delta_d(t-j) \\ \Delta_q(t+1) = \eta_q^{j+1}\Delta_q(t-j) \end{cases} \tag{37}$$

The cost index of the MSET-CCSMPCC can be constructed as follows.

$$\begin{aligned} J_{M\Delta}(t) = &\sum_{j=0}^{m-1} \lambda_{dj}(\Delta_d(t-j)\eta_d^{j+1} - \Delta_d(t+1))^2 \\ &+ \sum_{j=0}^{m-1} \lambda_{qj}(\Delta_q(t-j)\eta_q^{j+1} - \Delta_q(t+1))^2 \end{aligned} \tag{38}$$

Where $\Delta_d(t-j) = i_d^*(t-j) - i_d(t-j)$, $\Delta_q(t-j) = i_q^*(t-j) - i_q(t-j)$, and $\Delta_d(t+1)$, $\Delta_q(t+1)$ can be derived by combining (27) and (35). Assuming that each sub-item has

the same weight, λ_{dj} and λ_{qj} can be chosen as 1. By solving $\frac{\partial J_{M\Delta}(t)}{\partial u_d^*(t)} = 0$ and $\frac{\partial J_{M\Delta}(t)}{\partial u_q^*(t)} = 0$, the cost index $J_{M\Delta}(t)$ in (38) is minimized, and the appropriate voltage variables $u_d^*(t)$ and $u_q^*(t)$ can be calculated as

$$\begin{cases} u_d^*(t) = \dfrac{L}{mT_c}(mi_d^*(t+1) - \displaystyle\sum_{j=0}^{m-1} \eta_d^{j+1} i_d^*(t-j) \\ \quad -(mi_d(t) - \displaystyle\sum_{j=0}^{m-1} \eta_d^{j+1} i_d(t-j)) - mT_c\hat{n}_d(t)) \\ u_q^*(t) = \dfrac{L}{mT_c}(mi_q^*(t+1) - \displaystyle\sum_{j=0}^{m-1} \eta_q^{j+1} i_q^*(t-j) \\ \quad -(mi_q(t) - \displaystyle\sum_{j=0}^{m-1} \eta_q^{j+1} i_q(t-j)) - mT_c\hat{n}_q(t)) \end{cases} \tag{39}$$

In Fig. 3, the block diagram of the MSET-CCSMPCC is depicted.

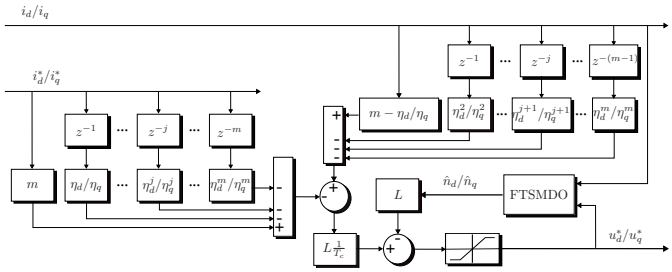

Fig. 3. Block diagram of the MSET-CCSMPCC.

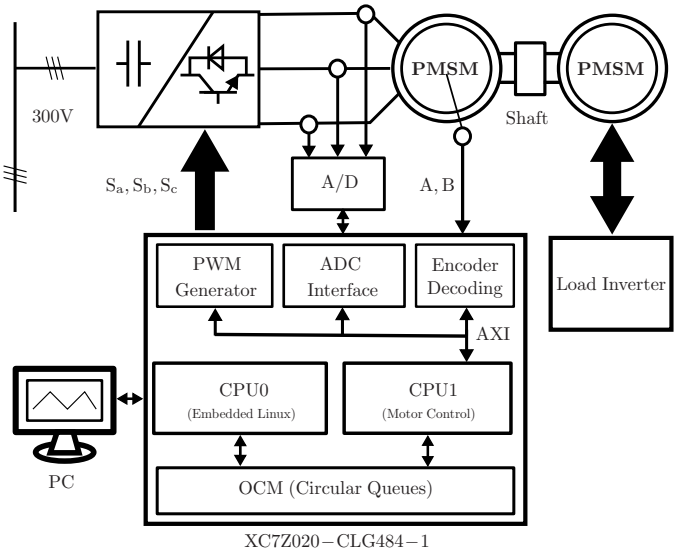

Fig. 4. Block diagram of the designed FPGA-based hardware system.

IV. Experimental Results

An FPGA-based hardware system has been designed as shown in Fig. 4. The XC7Z020-CLG484-1, which incorporates dual-core Cortex-A9 processors and an FPGA core, was utilized as the control unit. A pulse-width modulation (PWM) Generator, an analog-to-digital converter (ADC) interface, an Encoder Decoding are implemented on the FPGA core by employing verilog language. By properly designing the PWM Generator module clock, a desired resolution is achieved. A parallel interface is designed to interface to a 16-bit, simultaneous sampling ADC AD7606. The Encoder Decoding is designed to interface to an incremental encoder, which provides information on the sensor's current position and the period between two encoder events. CPU0 (CPU: central processing unit), which runs an embeded linux, communicates with a control and monitoring software installed on the computer via Ethernet. The motor control algorithms are implemented on the CPU1, which communicates with the CPU0 via the on chip memory (OCM).

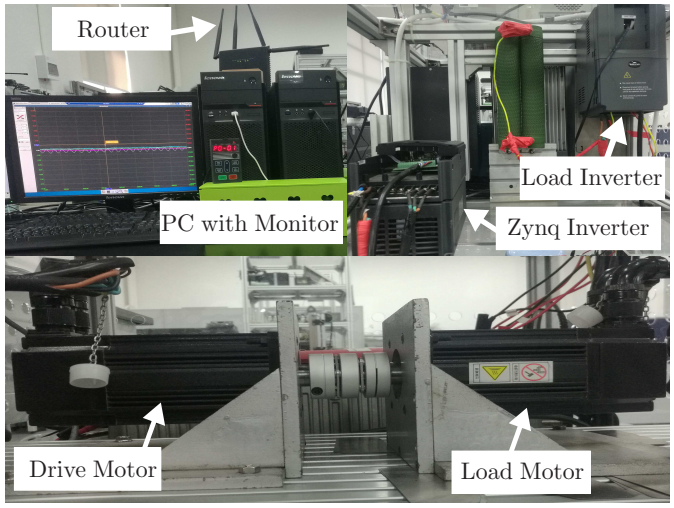

Fig. 5. Experimental setup description.

To verify the proposed algorithms, an SPMSM test bench has been established as shown in Fig. 5. Two SPMSMs made by Wenling Yuhai Electromechanical Corporation with the parameters specified in Table I are coupled via a flexible coupling. The drive motor which is driven by an FPGA-based hardware system, is used to test the algorithms. And the load motor which is driven by a 3.0 kW commercial inverter made by Micno Corporation, is applied to provide the speed. An incremental encoder with a resolution of 2500 pulses per revolution (P/R) is utilized for measuring the SPMSM speed. Three high precision sampling resistors are used to measure the stator currents.

In the following sections, experimental results are presented and analyzed. In the section A, the proposed methods are tested to verify the effectiveness. In the section B, the performances of the designed FTSMDO are verified. In the section C and D, the proposed methods are explicitly compared with the existed conventional CCS-MPCC for sharing the advantages and drawbacks.

A. Speed Reversal Performance

Experiments to validate the performances of the EXM-CCSMPC and MSET-CCSMPCC during the rated full-speed

TABLE I
PARAMETERS OF SPMSM

Descriptions	Parameters	Nominal Values
Stator resistance	R	1.7912 Ω
Stator inductance	L	3.5 mH
Pole pairs	p	4
PM flux	λ	0.0799 Vs
Rated power	P_N	0.75 kW
Rotor inertia	J_n	0.00024 $Kg \cdot m^2$
Rated current	I_N (eff.)	3.5 A
Rated speed	ω_{MN}	3000 rpm
Rated voltage	U_N (eff.)	220 V
Rated torque	T_{MN}	2.4 Nm
DC link voltage	V_{dc}	300 V

range are carried out respectively in Figs. 7 and 6, where the load motor is out of service and the ω_m^* is directly changed in the program. In both experiments, the PI control with the same parameters is applied to the outer speed loop, and the given speed ω_m^* is changed from 3000 rpm to -3000 rpm at 0.16s. The q-axis currents of both methods jump to their upper bounds within 3 ms, but the i_q overshoot of MSET-CCSMPCC (almost no overshoot) is much smaller than that of EXM-CCSMPC (0.8A overshoot). As i_q is proportional to the electromagnetic torque, the drive SPMSM reverses from 3000 rpm to -3000 rpm fast in both experiments (within 0.09s). The experimental results indicate the proposed EXM-CCSMPCC and MSET-CCSMPCC have fast dynamic response in the full-speed range. However, the MSET-CCSMPCC has better performance considering the overshoot suppression.

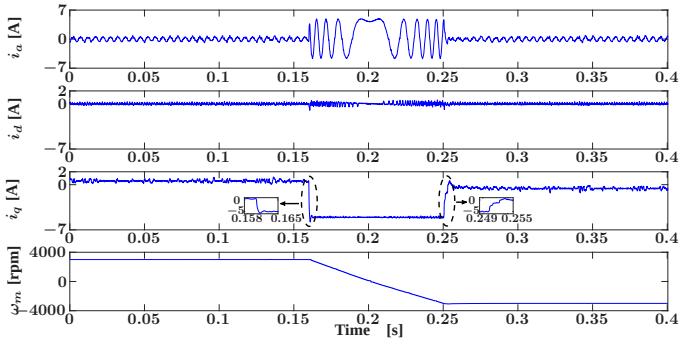

Fig. 6. Experimental results during the rated full-speed reversal process. (PI cascade with EXM-CCSMPC, from 3000 rpm to -3000 rpm).

B. Performance of FTSMDO

To verify the excellent performances of the designed FTSMDO, an exponential reaching law based SMDO is given below as a comparison method.

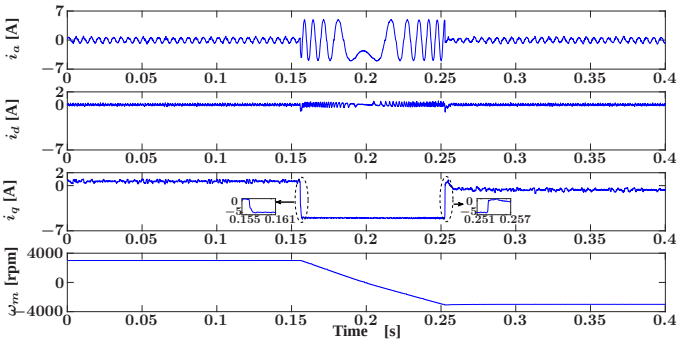

Fig. 7. Experimental results during the rated full-speed reversal process. (PI cascade with MSET-CCSMPCC, from 3000 rpm to -3000 rpm).

$$\begin{cases} \dot{\hat{i}}_q = \dfrac{u_q^*}{L} + \hat{n}_q + \alpha_q e_q + \beta_q \text{sign}(e_q) \\ \dot{\hat{n}}_q = \alpha_{nq}(\alpha_q e_q + \beta_q \text{sign}(e_q)) \end{cases} \tag{40}$$

Experiments to validate the performances of the SMDO and FTSMDO during the i_q step response test are carried out in Figs. 8 and 9, where the i_q^* is directly changed in the program and the motor speed is provided by the Micno commercial inverter. The conventional CCS-MPCC is applied to the current loop of the FPGA-based hardware system, and the i_q and u_q^* are fed back to the SMDO and FTSMDO respectively. The drive motor runs at 450 rpm, and the i_q^* is changed from 0A to 5A. It can be seen that the FTSMDO tracks slightly faster than the SMDO, and the $\hat{n}_q$ and $\hat{i}_q$ of the SMDO have more serious chatter than that of the FTSMDO (approximately 2 times larger).

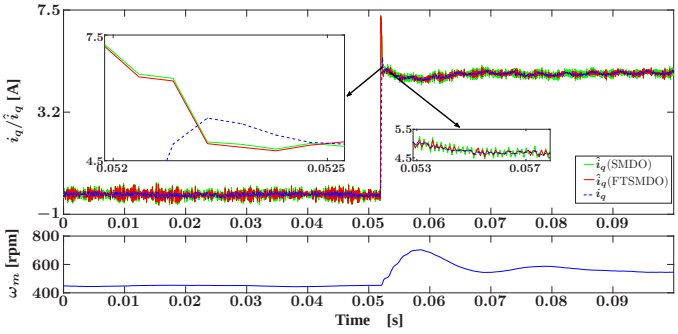

Fig. 8. The $\hat{i}_q$ experimental results of the FTSMDO and SMDO under the i_q step response test with the conventional DPCC. (450 rpm, i_q alters from 0A to 5A).

C. I_q Step Response Performance

The i_q step response performances of the conventional CCS-MPCC, EXM-CCSMPCC, SSET-CCSMPCC and MSET-CCSMPCC are evaluated in Figs. 10, 11, 12 and 13 respectively, where the i_q^* is directly changed in the program and the motor speed is provided by the Micno commercial inverter. It can be seen that the SSET-CCSMPCC tracks more slowly (2ms approximately) than three other methods (within 1ms). However, both the conventional CCS-MPCC and EXM-CCSMPCC have overshoots. The overshoot of the i_q is

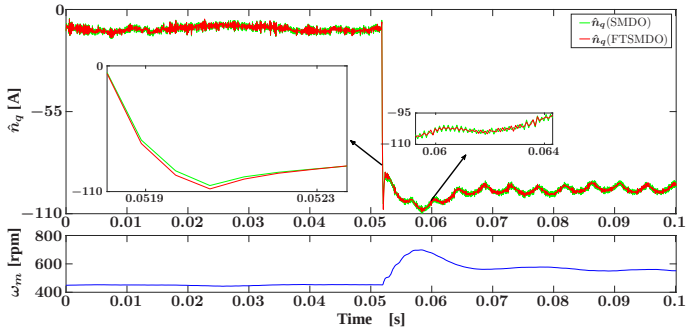

Fig. 9. The $\hat{n}_q$ experimental results of the FTSMDO and SMDO under the i_q step response test with the conventional DPCC. (450 rpm, i_q alters from 0A to 5A).

eliminated with the proposed SSET-CCSMPCC and MSET-CCSMPCC methods in the 0-2A, 2-4A, 4-0A and 0-5A step response tests. The proposed EXM-CCSMPCC and MSET-CCSMPCC have comparatable steady-state performances and the current variations are smaller than 0.28A when the i_q operates at 5A. The current variations of the SSET-CCSMPCC (0.32A when the i_q operates at 5A) and the conventional CCS-MPCC (0.3A when the i_q operates at 5A) are larger than those of two other methods.

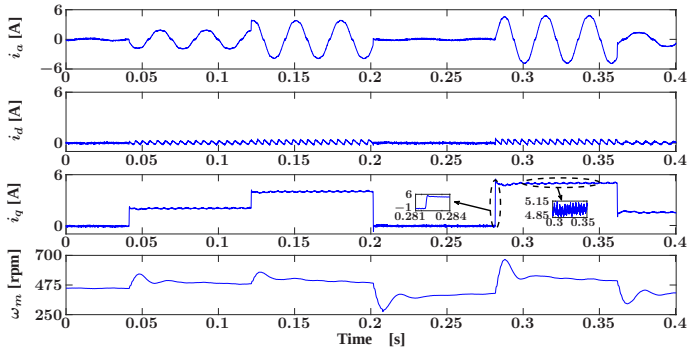

Fig. 10. Experimental results of the i_q step response test. (With the conventional CCS-MPCC, 450 rpm).

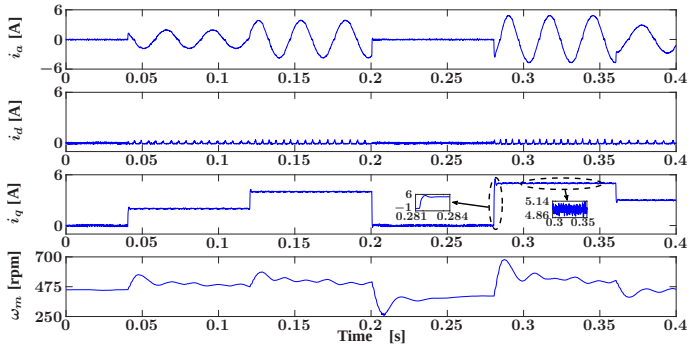

Fig. 11. Experimental results of the i_q step response test. (With the EXM-CCSMPCC, 450 rpm).

D. Parameter Sensitivity Evaluation

From (30) and (39), the proposed EXM-CCSMPCC and MSET-CCSMPCC are only affected by the stator inductance,

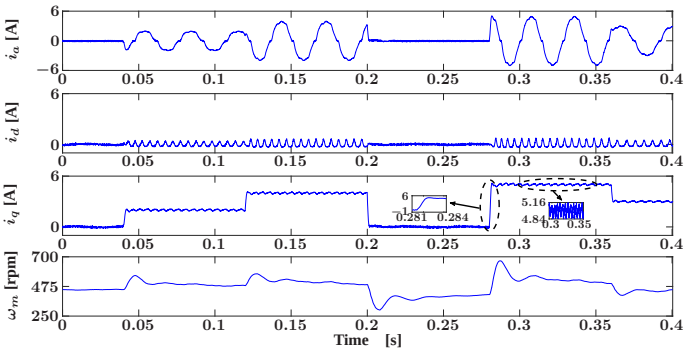

Fig. 12. Experimental results of the i_q step response test. (With the SSET-CCSMPCC, 450 rpm).

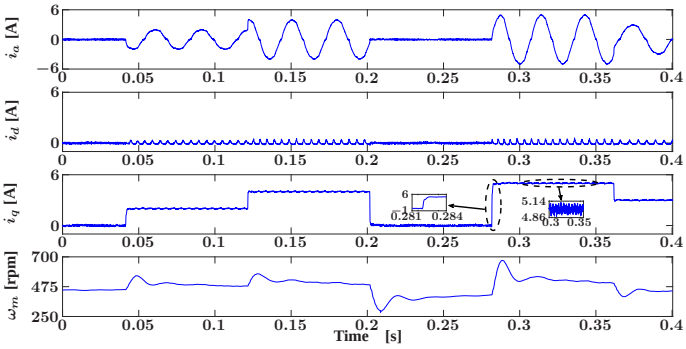

Fig. 13. Experimental results of the i_q step response test. (With the MSET-CCSMPCC, 450 rpm).

while the conventional CCS-MPCC is influenced by the stator inductance, stator resistance and permanent magnet flux linkage. Fig. 14 shows the experimental results of the conventional CCS-MPCC, where the feedback i_q decreases with the decreasing of the stator inductance. Figs. 15 and 16 compare the steady-state performances of the proposed EXM-CCSMPCC and MSET-CCSMPCC under the stator inductance variation. In the whole range of the inductance variation, the i_q keeps the average value of 5A with both methods. The stator inductance jumps to 9mH at 0.05s, the i_q of the EXM-CCSMPCC has a large chatter for the later 0.1s, while that of the MSET-CCSMPCC first jumps to 7A but returns to 5A fast. When the stator inductance deceases from 6mH to 2.62mH, the i_q variations of both methods are within 0.28A. When the inductance deceases from 2.62mH to 0.5mH, the i_q ripples increase, but the i_q ripples of the MSET-CCSMPCC increase more rapidly than that of the EXM-CCSMPCC.

V. Conclusion

This paper has proposed a robust continuous control set model-based predictive current control method for an SPMSM. An extended SPMSM model and a fast terminal sliding mode disturbance observer are considered for disturbance compensation. Furthermore, a multi-step error tracking CCS-MPCC is proposed to reduce the overshoot while keeping excellent steady-state and dynamic response performances. The experimental results implemented on an FPGA-based hardware verify the effectiveness of the proposed methods. The further work is to improve the algorithm robustness in a wider range of inductance variations.

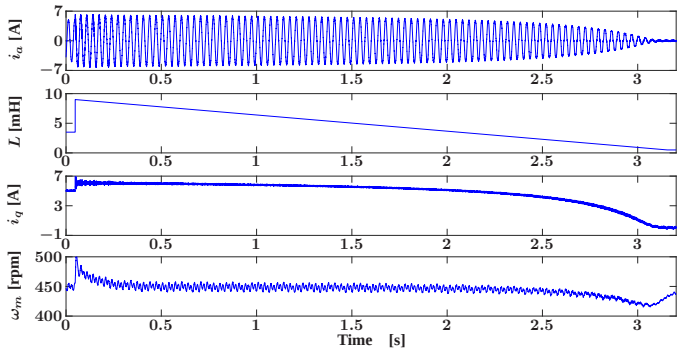

Fig. 14. The steady-state performance under the stator inductance variation. (With the conventional CCS-MPCC, 450 rpm, 5A i_q).

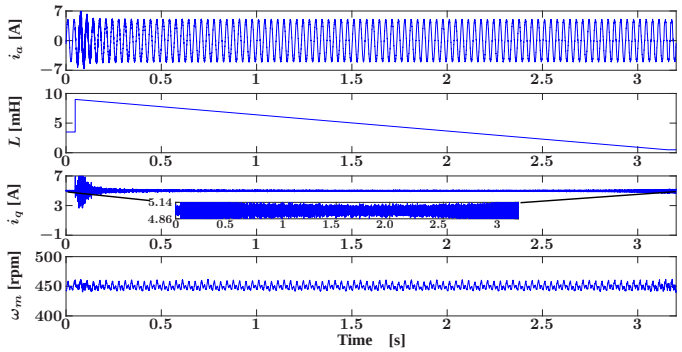

Fig. 15. The steady-state performance under the stator inductance variation. (With the EXM-CCSMPCC, 450 rpm, 5A i_q).

REFERENCES

[1] J. Yang, W. Chen, S. Li, L. Guo, and Y. Yan, "Disturbance/uncertainty estimation and attenuation techniques in pmsm drives-a survey," *IEEE Transactions on Industrial Electronics*, vol. 64, no. 4, pp. 3273–3285, April 2017.

[2] S. A. Odhano, P. Pescetto, H. A. A. Awan, M. Hinkkanen, G. Pellegrino, and R. Bojoi, "Parameter identification and self-commissioning in ac motor drives: A technology status review," *IEEE Transactions on Power Electronics*, vol. 34, no. 4, pp. 3603–3614, April 2019.

[3] J. Chen, J. Li, and R. Qu, "Maximum-torque-per-ampere and magnetization-state control of a variable-flux permanent magnet machine," *IEEE Transactions on Industrial Electronics*, vol. 65, no. 2, pp. 1158–1169, Feb 2018.

[4] S.-H. Chang and P.-Y. Chen, "Self-tuning gains of pi controllers for current control in a pmsm," in *2010 5th IEEE Conference on Industrial Electronics and Applications*, June 2010, pp. 1282–1286.

[5] A. D. Alexandrou, N. K. Adamopoulos, and A. G. Kladas, "Development of a constant switching frequency deadbeat predictive control technique for field-oriented synchronous permanent-magnet motor drive," *IEEE Transactions on Industrial Electronics*, vol. 63, no. 8, pp. 5167–5175, Aug 2016.

[6] B. Wang, Z. Dong, Y. Yu, G. Wang, and D. Xu, "Static-errorless deadbeat predictive current control using second-order sliding-mode disturbance observer for induction machine drives," *IEEE Transactions on Power Electronics*, vol. 33, no. 3, pp. 2395–2403, March 2018.

[7] M. Siami, D. A. Khaburi, M. Rivera, and J. Rodriguez, "An experimental evaluation of predictive current control and predictive torque control for a pmsm fed by a matrix converter," *IEEE Transactions on Industrial Electronics*, vol. 64, no. 11, pp. 8459–8471, Nov 2017.

[8] F. Wang, S. Li, X. Mei, W. Xie, J. Rodriguez, and R. M. Kennel, "Model-based predictive direct control strategies for electrical drives: An experimental evaluation of ptc and pcc methods," *IEEE Transactions on Industrial Informatics*, vol. 11, no. 3, pp. 671–681, June 2015.

[9] B.-J. Kang and C.-M. Liaw, "A robust hysteresis current-controlled pwm inverter for linear pmsm driven magnetic suspended positioning system," *IEEE Transactions on Industrial Electronics*, vol. 48, no. 5, pp. 956–967, Oct 2001.

[10] Y. Zhang, L. Huang, D. Xu, J. Liu, and J. Jin, "Performance evaluation of two-vector-based model predictive current control of pmsm drives," *Chinese Journal of Electrical Engineering*, vol. 4, no. 2, pp. 65–81, June 2018.

[11] A. A. Ahmed, B. K. Koh, and Y. I. Lee, "A comparison of finite control set and continuous control set model predictive control schemes for speed control of induction motors," *IEEE Transactions on Industrial Informatics*, vol. 14, no. 4, pp. 1334–1346, April 2018.

[12] Y. Yan, J. Yang, Z. Sun, C. Zhang, S. Li, and H. Yu, "Robust speed regulation for pmsm servo system with multiple sources of disturbances via an augmented disturbance observer," *IEEE/ASME Transactions on Mechatronics*, vol. 23, no. 2, pp. 769–780, April 2018.

[13] B. Wang, X. Chen, Y. Yu, G. Wang, and D. Xu, "Robust predictive current control with online disturbance estimation for induction machine drives," *IEEE Transactions on Power Electronics*, vol. 32, no. 6, pp. 4663–4674, June 2017.

[14] P. K. Nandam and P. C. Sen, "A comparative study of a luenberger observer and adaptive observer-based variable structure speed control system using a self-controlled synchronous motor," *IEEE Transactions on Industrial Electronics*, vol. 37, no. 2, pp. 127–132, April 1990.

[15] S. Lin, Y. Cai, B. Yang, and W. Zhang, "Electrical line-shafting control for motor speed synchronisation using sliding mode controller and disturbance observer," *IET Control Theory Applications*, vol. 11, no. 2, pp. 205–212, 2017.

[16] X. Zhang, L. Sun, K. Zhao, and L. Sun, "Nonlinear speed control for pmsm system using sliding-mode control and disturbance compensation techniques," *IEEE Transactions on Power Electronics*, vol. 28, no. 3, pp. 1358–1365, March 2013.

[17] X. Zhang, B. Hou, and Y. Mei, "Deadbeat predictive current control of permanent-magnet synchronous motors with stator current and disturbance observer," *IEEE Transactions on Power Electronics*, vol. 32, no. 5, pp. 3818–3834, May 2017.

[18] Y. Jiang, W. Xu, C. Mu, and Y. Liu, "Improved deadbeat predictive current control combined sliding mode strategy for pmsm drive system," *IEEE Transactions on Vehicular Technology*, vol. 67, no. 1, pp. 251–263, Jan 2018.

[19] Y. Feng, X. Yu, and F. Han, "High-order terminal sliding-mode observer for parameter estimation of a permanent-magnet synchronous motor," *IEEE Transactions on Industrial Electronics*, vol. 60, no. 10, pp. 4272–4280, Oct 2013.

[20] L. Fridman and A. Levant, *High order sliding modes as the natural phenomenon in control theory*, 01 1996, vol. 217, pp. 107–133.

[21] J. Han, "From pid to active disturbance rejection control," *IEEE Transactions on Industrial Electronics*, vol. 56, no. 3, pp. 900–906, March 2009.

[22] M. Iqbal, A. I. Bhatti, S. I. Ayubi, and Q. Khan, "Robust parameter estimation of nonlinear systems using sliding-mode differentiator observer," *IEEE Transactions on Industrial Electronics*, vol. 58, no. 2, pp. 680–689, Feb 2011.

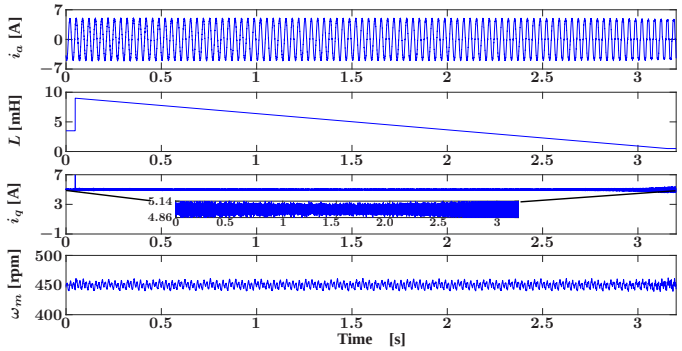

Fig. 16. The steady-state performance under the stator inductance variation. (With the MSET-CCSMPCC, 450 rpm, 5A i_q).